Thermal Decomposition of Tetramethyl Orthosilicate in the Gas Phase: An Experimental and Theoretical Study of the Initiation Process

J. C. S. Chu, R. Soller, and M. C. Lin*

Department of Chemistry, Emory University, Atlanta, Georgia 30322

C. F. Melius*

Combustion Research Facility, Sandia National Laboratories, Livermore, California 94552

Received: July 27, 1994; In Final Form: October 26, 1994[⊗]

The thermal decomposition of $Si(OCH_3)_4$ (TMOS) has been studied by FTIR at temperatures between 858 and 968 K. The experiment was carried out in a static cell at a constant pressure of 700 Torr under highly diluted conditions. Additional experiments were performed by using toluene as a radical scavenger. The species monitored included TMOS, CH_2O, CH_4, and CO. According to these measurements, the first-order global rate constants for the disappearance of TMOS without and with toluene can be given by $k_g = 1.4 \times 10^{16} \exp(-81\,200/RT)\ s^{-1}$ and $k_g = 2.0 \times 10^{14} \exp(-74\,500/RT)\ s^{-1}$, respectively. The noticeable difference between the two sets of Arrhenius parameters suggests that, in the absence of the inhibitor, the reactant was consumed to a significant extent by radical attacks at higher temperatures. The experimental data were kinetically modeled with the aid of a quantum-chemical calculation using the BAC-MP4 method. The results of the kinetic modeling, using the mechanism constructed on the basis of the quantum-chemical data and the known C/H/O chemistry, identified two rate-controlling reactions: TMOS → $CH_3OH + (CH_3O)_2SiOCH_2$ (reaction 2) and $CH_2OSi(OCH_3)_3 \rightarrow CH_2O + Si(OCH_3)_3$ (reaction 3), which have the following respective first-order rate constants, given in the units of s^{-1}: $k_2 = 1.6 \times 10^{14} \exp(-74\,000/RT)$ and $k_3 = 3.8 \times 10^{14} \exp(-60\,000/RT)$. In addition to these new kinetic data, the heats of formation of many relevant $SiO_xC_yH_z$ species computed with the BAC-MP4 method are presented herein.

Introduction

Recently there has been considerable interest in the chemistry of tetraalkyl orthosilicates, particularly with respect to the deposition of SiO_2 insulating films using tetraethyl orthosilicate and other larger members of the homolog.[1−8] Most of these studies were carried out on solid surfaces and often involved the interaction of various silicate molecules with hydroxyl groups on the surface.[9,10]

In order to understand the basic thermochemistry of the $Si(OR)_4$ molecules, we have recently investigated the kinetics of the thermal decomposition of tetramethyl orthosilicate (TMOS) and tetraethyl orthosilicate (TEOS) in the gas phase by Fourier transform infrared (FTIR) spectrometry. Time-resolved concentration profiles of the reactants and major products were measured as functions of temperature and the partial pressure of the reactants. The preliminary results of this study[11] indicate that TMOS decays with an apparent global first-order rate constant, $k_g = 1.4 \times 10^{16} \exp(-81\,200/RT)\ s^{-1}$, which differs considerably from that for TEOS, $k_g = 7.4 \times 10^{10} \exp(-49\,500/RT)\ s^{-1}$, where $R = 1.987$ cal/(mol·deg). At 800 K, TMOS is 2400 times more stable than TEOS. This result clearly suggests that TEOS, which possesses β-hydrogens, is capable of undergoing a molecular elimination reaction producing C_2H_4 and other stable intermediates. Such a low-energy reaction path, on the other hand, is not available for TMOS.[11]

To fully elucidate the mechanism of the TMOS decomposition reaction as well as to determine the amount of energy required to break the C−O or the Si−O bond as mentioned above, we have carried out additional kinetic measurements using toluene as a radical scavenger. These new and earlier kinetic data have been kinetically modeled by using a comprehensive set of reactions based on the thermochemical data predicted by the BAC-MP4 (bond-additivity-corrected Møller−Plesset fourth-order perturbation) method.[12,13] The results of this new study reported herein reveal for the first time the intricate and fascinating fragmentation chemistry of TMOS, which is much different from that of TEOS and other tetraalkyl orthosilicates containing β-hydrogens.

Experimental Section

The thermal decomposition of TMOS was performed in a quartz static cell with a volume of ~270 cm^3. This reactor was placed in a double-walled cylindrical furnace. The furnace temperature was controlled to ±0.5 K with a solid-state temperature controller (Omega CN-9000), and it was monitored through a thermocouple (K type) inserted in a small tube sealed at the center of the reactor.

The pyrolyzed and unpyrolyzed samples were analyzed by FTIR spectrometry (Mattson Polaris) using a 15 cm long, 2.5 cm o.d. sample cell sealed with two KCl windows. This cell was directly attached to the reactor and associated vacuum system with 9.5 mm o.d. Teflon tubing. The vacuum system was pumped with a diffusion pump (Varian Co., HS-10) to about at 10^{-5} Torr base pressure before each run to eliminate any possible impurities (H_2O, CO_2).

The reactant TMOS (Aldrich, 99.9+%) and C_7H_8 (Fisher, reagent grade) were further purified *in vacuo* by trap-to-trap distillation using appropriate slush baths to eliminate H_2O and other impurities. The reactant concentrations were varied from 0.6 to 1.4% for TMOS without toluene and fixed at 0.16% with toluene inhibition experiments. Argon (SGS, UHP grade) was used as the buffer gas for all of the experiments without further

[⊗] Abstract published in *Advance ACS Abstracts*, December 1, 1994.

0022-3654/95/2099-0663$09.00/0

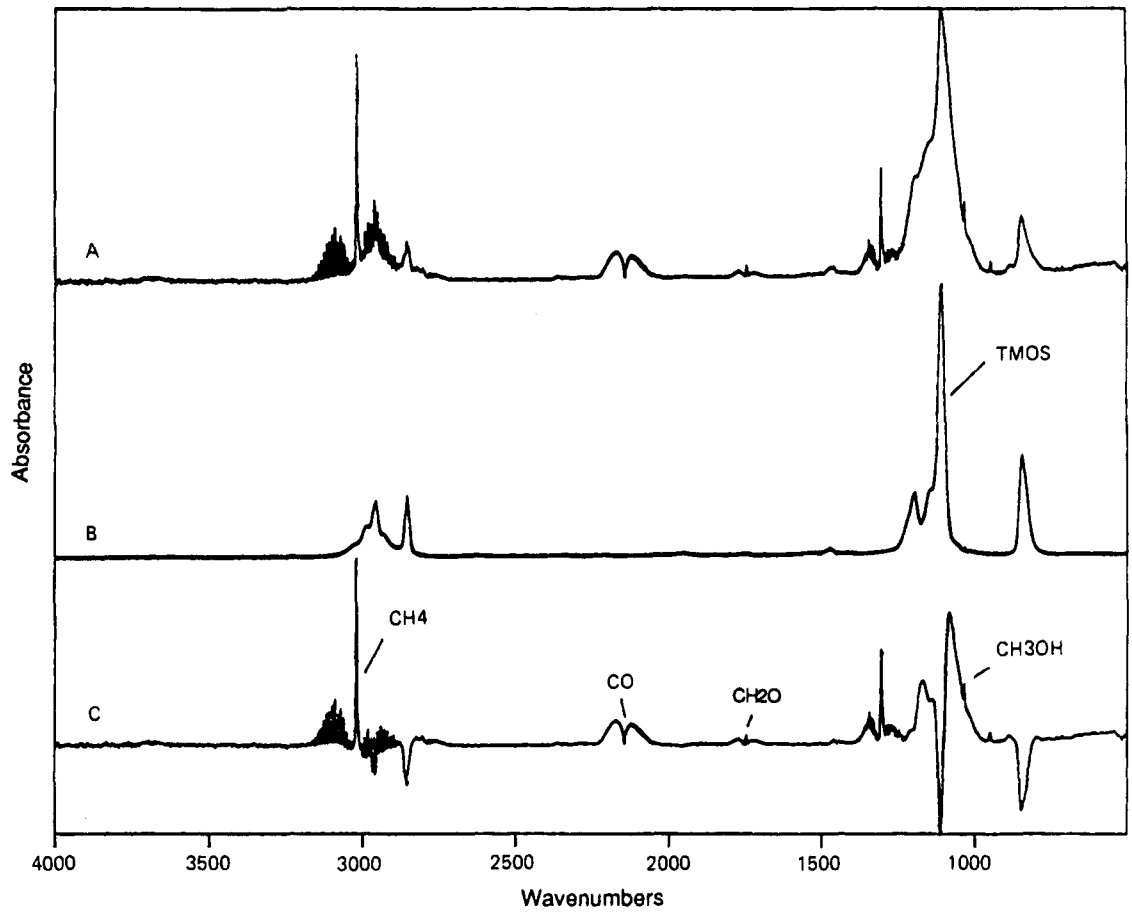

Figure 1. TMOS FTIR spectra (without C_7H_8 scavenger): (A) 0.6% TMOS/Ar mixture pyrolyzed at 705 Torr and T = 940 K for 6 min; (B) unpyrolyzed 0.6% TMOS/Ar mixture; (C) the difference between parts A and B.

purification. Pyrolysis was carried out between 858 and 968 K without inhibition and between 866 and 984 K with inhibition. The reaction time usually ran from several minutes to several hours. The reaction pressures were kept constant near atmospheric pressure in order to reduce possible reactor wall effects.

The reaction products identified in the inhibitor-free experiment by FTIR spectrometry were CH_4, CO, CH_2O, and CH_3OH. A typical set of spectra for the pyrolyzed and unpyrolyzed samples is shown in Figure 1. The major peaks of the various key products and the reactant mentioned have been identified on the spectra. Spectra of the C_7H_8-inhibited reaction are presented in Figure 2. Toluene effectively reduced all major products labeled in Figure 1. The concentrations of the major products in the thermal decomposition reaction were calibrated with more than 10 sets of mixtures composed of varying amounts of the reactant and products. The pressures of the calibration samples (~280 Torr) were always kept the same as those of the expanded reaction mixtures in the absorption cell. In this manner, the effect of pressure (Lorentz) broadening can be properly corrected.

In order to elucidate the reaction mechanism, the measured time-resolved concentration profiles of the reactant and products have been kinetically modeled with the CHEMKIN program.[14] Since the Si chemistry and kinetics relevant to the present system are nonexistent in the literature, our mechanism was guided extensively by the results of a quantum-chemical calculation using the BAC-MP4 method.[12,13] To facilitate the calculations, dimethyl orthosilicate, $(CH_3O)_2Si(OH)_2$, was employed as the model compound. The reactions and their associated rate constants for C/H/O species were based mostly on those recommended by Tsang.[15,16] The mechanism used in our final simulation is summarized in Table 1.

Results

A. Kinetic Data. The thermal decomposition reaction of TMOS without toluene inhibition was studied at temperatures between 858 and 968 K at a constant total pressure of 700 Torr, using three different mixtures diluted with Ar (0.6%, 1.0% and 1.4%). In addition, a 0.16% TMOS sample with 3.2% toluene was employed in the inhibition experiment using 780 Torr of the mixture. The rates of TMOS disappearance in both studies were found to be approximately first order, as illustrated in Figures 3 and 4. From the slopes of these first-order TMOS decay plots, one can evaluate the apparent global first-order rate constant for the reaction

$$Si(OCH_3)_4 \xrightarrow{k_g} SiO_2, CH_3OH, CH_2O, C_2H_4, CO, H_2, \text{etc.}$$

The apparent global first-order rate constants for the $Si(OCH_3)_4$ decomposition reaction with and without toluene inhibition are shown in Figure 5. The k_g values can be expressed in terms of the least-squares-fitted Arrhenius equations:

$$k_g = 10^{16.15\pm0.35} \exp((-81\,200 \pm 1600)/RT)\ s^{-1} \quad (\text{w/o } C_7H_8) \quad (I)$$

$$k_g = 10^{14.30\pm0.35} \exp((-74\,460 \pm 1500)/RT)\ s^{-1} \quad (\text{with } C_7H_8) \quad (II)$$

The errors given above represent one standard deviation. The much smaller values of the A factor and the activation energy for the rate constant with toluene inhibition are most interesting. Since the formation of small molecular products, such as CO,

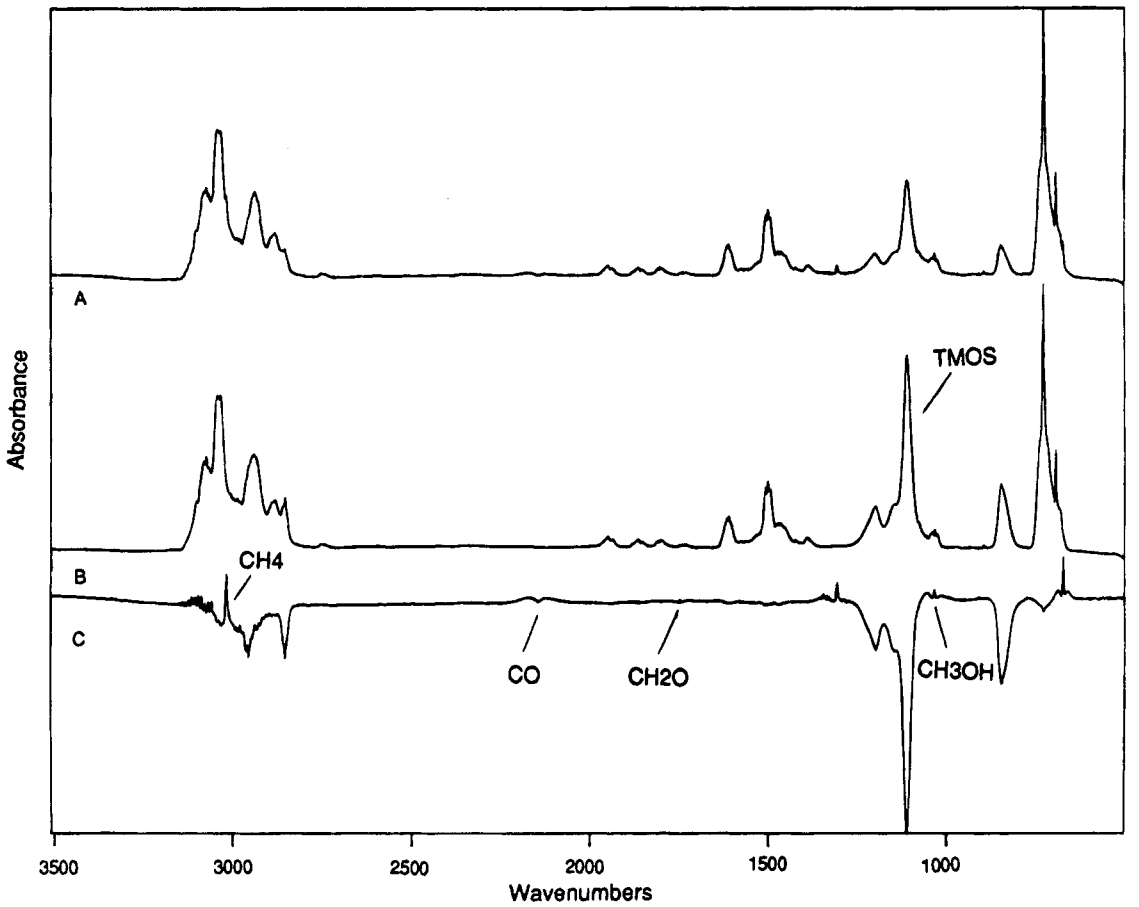

Figure 2. TMOS FTIR spectra (with C_7H_8 scavenger): (A) 0.16% TMOS + 3.2% C_7H_8/Ar mixture pyrolyzed at 770 Torr and T = 937 K for 6 min; (B) unpyrolyzed 0.16% TMOS + 3.2% C_7H_8/Ar mixture; (C) the difference between parts A and B.

CH_2O, and CH_4, was significantly reduced by the inhibition of toluene, the reactant appeared to be consumed, at least in part, by radical attacks. The inhibition effect is most vividly illustrated by the spectral data presented in Figures 1 and 2. Six sets of data obtained from pyrolyses of different mixtures at different temperatures, with and without toluene inhibition, are plotted as a function of time and compared with the kinetically modeled values in Figures 6 and 7.

Since these products were formed mostly by secondary and other late-stage reactions, no effort was made to model the rate constants of other reaction steps except for reactions 2 and 3, which were based only on the global TMOS decay rates with and without added toluene. Although CH_3OH derives in part from reaction 2, which is a primary process, the strong overlap of the C−O stretching frequency with that of the intense parent C−O stretching mode near 1000 cm^{-1} makes the quantitative determination and utilization of its growth kinetics impossible.

B. Quantum-Chemical Calculation with the BAC-MP4 Method. To date, very little information is available on the thermochemistry and the stabilities of the whole class of $Si(OR)_4$ molecules, where R = alkyl. In a separate paper,[12] we present the heats of formation and bond dissociation energies for the $Si(OR)_4$ compounds. In this paper, we present the thermochemistry appropriate for the TMOS decomposition, which includes rather unusual reaction intermediates. The thermochemistry is based on quantum chemical calculations using the technique of BAC-MP4 developed by Melius and Binkley.[13] This technique has been applied extensively and successfully for its reliable prediction of the thermochemistry of C/H/N/O species[13,17,18] and silicon-containing species.[12,19,20] The results of the present calculation for the heats of formation of various related, smaller analogs, which are theoretically more manageable with a present-day computer, are summarized in Table 2. From these thermochemical data, we can estimate the strength of various chemical bonds which are relevant to the present system. For example, the great strength of the $CH_3-OSi(OH)_3$ bond, 98.4 kcal/mol, and the $CH_3O-Si(OH)_3$ bond, 131.2 kcal/mol (see Table 3), rules out the importance of the unimolecular fragmentation of TMOS via the breaking of these bonds under the conditions employed in the present study. Accordingly, a new low-energy reaction path was explored theoretically. Such a low-energy decomposition channel was identified by using $(CH_3O)_2Si(OH)_2$ as a model; this reaction channel involves a molecular elimination process occurring via a proton transfer transition state;

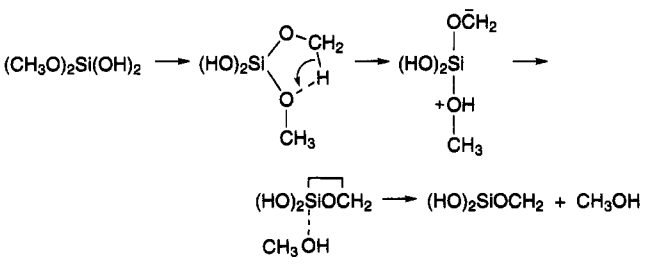

The zwitterionic transition state intermediate is unstable and closes to form a three-membered ring. The CH_3OH is then eliminated to produce the molecular product, CH_3OH, and the ring intermediate. The energy diagram of this reaction is schematically presented in Figure 8. The most interesting aspect of the mechanism, aside from the formation of the three-membered ring product, $(HO)_2\overline{SiOCH_2}$, as depicted in the figure, is the revelation that the ring molecule can form an association

TABLE 1: Reaction Mechanism for TMOS Decomposition with and without Toluene Inhibition[a]

reactions considered	A	b	E
	Si Chemistry[b] (X = OCH_3)		
1. $SiX_4 \rightarrow CH_3 + OSiX_3$	5.00E+16[c]	0.0	94000[d]
2. $SiX_4 \rightarrow CH_3OH + CH_2OSiX_2$	1.60E+14	0.0	74000
3. $CH_2OSiX_3 \rightarrow CH_2O + SiX_3$	3.80E+14	0.0	60000
4. $H + SiX_4 \rightarrow H_2 + CH_2OSiX_3$	2.60E+13	0.0	4700
5. $OH + SiX_4 \rightarrow H_2O + CH_2OSiX_3$	1.60E+13	0.0	800
6. $CH_3 + SiX_4 \rightarrow CH_4 + CH_2OSiX_3$	1.00E+12	0.0	10000
7. $H + CH_2OSiX_3 \rightarrow SiX_4$	7.00E+13	0.0	0.0
8. $H + CH_2OSiX_2 \rightarrow SiX_3$	7.00E+13	0.0	0.0
9. $CH_2OSiX_2 \rightarrow C_2H_5OSi(O)X$	1.00E+13	0.0	20000
11. $C_2H_5OSi(O)X \rightarrow C_2H_4 + CH_3OH + SiO_2$	5.00E+13	0.0	60000
12. $H + CH_2OSi(O)X \rightarrow OSiX_2$	7.00E+13	0.0	0.0
13. $H + SiX_3 \rightarrow HSiX_3$	1.00E+13	0.0	0.0
14. $H + HSiX_3 \rightarrow H_2 + SiX_3$	1.30E+08	1.6	2100
15. $OSiX_3 \rightarrow OSiX_2 + CH_3O$	1.00E+14	0.0	54000
16. $SiX_3 \rightarrow CH_3 + OSiX_2$	1.00E+13	0.0	25000
17. $CH_2OSi(O)X \rightarrow CH_2O + CH_3 + SiO_2$	5.00E+13	0.0	53000
18. $OSiX_2 \rightarrow CH_3O + SiO_2 + CH_3$	3.00E+16	0.0	99000
19. $H + OSiX_2 \rightarrow H_2 + CH_2OSi(O)X$	2.00E+13	0.0	5000
20. $CH_3 + OSiX_2 \rightarrow CH_4 + CH_2(O)SiOX$	9.00E+12	0.0	10000
21. $CH_2OSiX_3 + C_7H_8 \rightarrow SiX_4 + C_7H_7$	5.50E+10	0.0	12000
	C/H/O Chemistry[e]		
22. $CH_3O + C_7H_8 \rightleftarrows CH_3OH + C_7H_7$	5.50E+10	0.0	12000
23. $CH_3 + C_7H_8 \rightleftarrows CH_4 + C_7H_7$	5.50E+11	0.0	12000
24. $H + C_7H_8 \rightleftarrows C_7H_7 + H_2$	8.10E+13	0.0	9200
25. $H + C_7H_8 \rightleftarrows C_6H_6 + CH_3$	1.20E+13	0.0	5156
26. $C_2H_5 + C_7H_8 \rightleftarrows C_2H_6 + C_7H_7$	1.70E+13	0.0	12600
27. $C_2H_3 + C_7H_8 \rightleftarrows C_2H_4 + C_7H_7$	1.70E+13	0.0	12600
28. $OH + C_7H_8 \rightleftarrows H_2O + C_7H_7$	1.70E+13	0.0	2600
29. $C_7H_8 \rightleftarrows C_7H_7 + H$	3.10E+15	0.0	89420
30. $C_2H_5 + M \rightleftarrows C_2H_4 + H + M$	2.94E+33	1.2	37440
31. $H + C_2H_4 \rightleftarrows H_2 + C_2H_3$	1.36E+06	2.5	12300
32. $C_2H_3 + M \rightleftarrows C_2H_2 + H + M$	4.10E+41	−7.5	45800
33. $C_7H_7 + C_7H_7 \rightleftarrows C_{14}H_{14}$	1.00E+12	0.0	0.0
34. $CH_3 + CH_2O \rightleftarrows CH_4 + HCO$	5.54E+03	2.81	5860
35. $HCO + M \rightleftarrows CO + H + M$	190E+17	−1.0	17000
36. $H + HCO \rightleftarrows H_2 + CO$	7.20E+13	0.0	0.0
37. $CH_3 + HCO \rightleftarrows CH_4 + CO$	1.20E+14	0.0	0.0
38. $CH_3 + CH_3 \rightleftarrows C_2H_6$	1.00E+15	−0.6	0.0
39. $CH_3O + CH_3O \rightleftarrows CH_2O + CH_3OH$	7.00E+13	0.0	0.0
40. $H + CH_3OH \rightleftarrows CH_2OH + H_2$	1.70E+07	2.1	4900
41. $CH_3 + CH_3OH \rightleftarrows CH_2OH + CH_4$	2.60E+09	3.2	7200
42. $OH + CH_3OH \rightleftarrows CH_2OH + H_2O$	1.00E+11	2.5	−960
43. $CH_2OH + M \rightleftarrows CH_2O + H + M$	4.50E+25	−2.5	34200
44. $H + CH_4 \rightleftarrows H_2 + CH_3$	2.30E+04	3.0	8800
45. $H + C_2H_6 \rightleftarrows H_2 + C_2H_5$	5.40E+02	3.5	5200
46. $CH_3 + C_2H_6 \rightleftarrows CH_4 + C_2H_5$	5.50E−01	4.0	8300
47. $CH_3OH \rightleftarrows CH_3 + OH$	1.90E+16	0.0	91800
48. $CH_3O + M \rightleftarrows CH_2O + H + M$	3.90E+37	−6.65	33270
49. $C_7H_8 + CH_2OH \rightleftarrows C_7H_7 + CH_3OH$	1.70E+13	0.0	12600
50. $CH_3OH \rightleftarrows CH_2 + H_2O$	3.00E+13	0.0	79000
51. $CH_2 + CH_3 \rightleftarrows C_2H_4 + H$	1.80E+13	0.0	0.0
52. $CH_3OH + H \rightleftarrows CH_3O + H_2$	1.40E+06	2.1	4900
53. $CH_3OH + CH_3 \rightleftarrows CH_3O + CH_4$	6.80+08	3.1	6950
54. $CH_3OH \rightleftarrows CH_2OH + H$	1.54E+16	0.0	96700
55. $CH_2O + H \rightleftarrows HCO + H_2$	1.30E+08	1.6	2200
56. $CH_2OH + HCO \rightleftarrows CH_3OH + CO$	1.20E+14	0.0	0.0
57. $CH_2OH + H \rightleftarrows CH_2O + H_2$	6.00E+12	0.0	0.0
58. $CH_2OH + CH_3 \rightleftarrows CH_2O + CH_4$	2.40E+12	0.0	0.0
59. $CH_2OH + CH_3 \rightleftarrows C_2H_5OH$	1.20E+13	0.0	0.0
60. $2CH_2OH \rightleftarrows CH_2O + CH_3OH$	4.80E+12	0.0	0.0
61. $HCO + CH_2OH \rightleftarrows 2CH_2O$	1.80E+14	0.0	0.0
62. $CH_2OH + C_2H_3 \rightleftarrows CH_2O + C_2H_4$	3.00E+13	0.0	0.0
63. $CH_2OH + C_2H_2 \rightleftarrows CH_2O + C_2H_3$	7.20E+11	0.0	9000
64. $CH_2OH + C_2H_5 \rightleftarrows CH_2O + C_2H_6$	2.40E+12	0.0	0.0
65. $H + CH_3O \rightleftarrows CH_2O + H_2$	2.00E+13	0.0	0.0
66. $H + CH_3 \rightleftarrows CH_4$	1.24E+15	−0.4	0.0
67. $H + C_2H_3 \rightleftarrows C_2H_2 + H_2$	9.64E+13	0.0	0.0
68. $CH_2O + M \rightleftarrows HCO + H + M$	1.20E+41	−6.9	96500
69. $CH_2O + M \rightleftarrows H_2 + CO + M$	8.20E15	0.0	69500

[a] Rate constants are given in the form of $k = AT^b e^{-E/RT}$ in units of mol, cm^3, s, and cal/mol. [b] All rate constants except k_2 and k_3, which have been kinetically modeled, were assumed on the basis of the their C/H/O analogs and the thermochemical data given in Tables 2 and 3. For example, the rate constants for TMOS + H and CH_3 were taken to be two times those for CH_3OH + H and CH_3. The arrows associated with these Si reactions indicate that they are irreversible. [c] Read as 5.00×10^{16}. [d] The value of $D[CH_3{-}OSi(OCH_3)_3]$ is lowered from 98.4 to 94.0 kcal/mol to account for the yields of CO and CH_2O. [e] See ref 15 and 16.

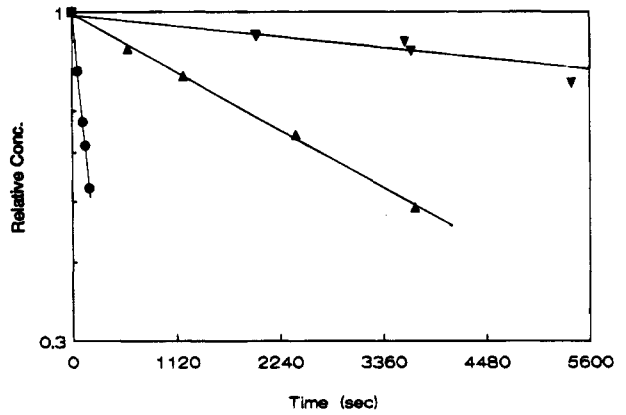

Figure 3. Apparent first-order decay plot of TMOS samples without C_7H_8 at various temperatures (●) 968 K; (▼) 915 K; (▲) = 940 K. The results are normalized, and the lines are least-squares fits.

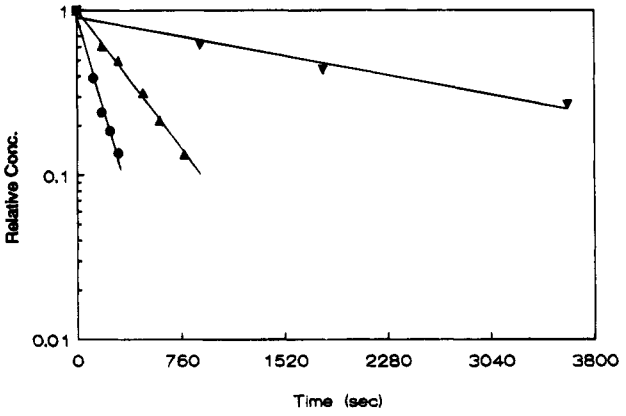

Figure 4. Apparent first-order decay plot of TMOS samples with C_7H_8 at various temperatures (●) 974 K; (▼) 874 K; (▲) = 907 K. The results are normalized, and the lines are least-squares fits.

complex with CH_3OH with a stability of about 10 kcal/mol. The complex is not stable under the experimental conditions employed, however.

Another interesting result from the BAC-MP4 calculation is that the ring product, $(HO)_2\overline{SiOCH_2}$, has a strong zwitterionic character. It has about the same heat of formation as its silicate isomer, $HOSi(O)OCH_3$ (see Figure 9). The isomerization should occur readily via a four-centered proton transfer:

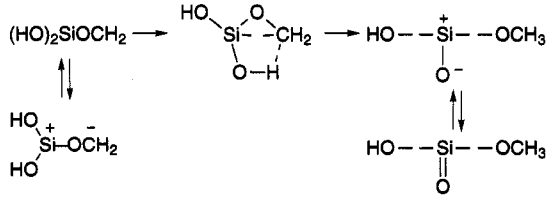

The isomerization should take place with facility under the high-temperature conditions used in the present study. On the other hand, the ring structure can open up to form the dative-bonded complex,

$$(HO)_2SiOCH_2 \rightarrow [(HO)_2Si \leftarrow OCH_2] \rightarrow Si(OH)_2 + CH_2O$$

which decomposes to produce a set of higher energy products, $Si(OH)_2 + CH_2O$. The reaction coordinate diagram for the $(HO)_2SiOCH_2$ system is shown in Figure 9. The mechanism, presented in Table 1 alluded to above, is based in part on the thermochemical results of Table 2.

Under the experimental conditions employed, the major early products of the TMOS decomposition reaction, CH_3OH and

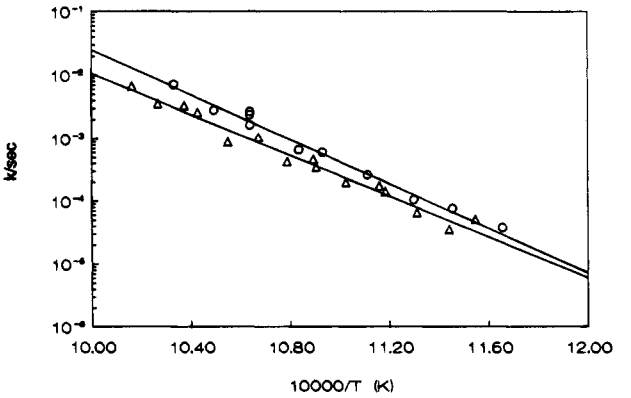

Figure 5. Comparison of the TMOS global decay rate constant with (triangles) and without (circles) C_7H_8 inhibition.

C_2H_4, are all comparatively stable. This accounts for the relatively minor effect of toluene on the global TMOS decay rates, as indicated in Figure 5. On the basis of these initiation processes and the C/H/O chemistry established from recent hydrocarbon and alcohol thermal decomposition and combustion chemistry,[15,16] we were able to assemble a reasonable set of reactions, as summarized in Table 1, to simulate the observed kinetic data. The results of this modeling, aided by sensitivity analyses with the SENKIN program,[22] are discussed in greater detail in the following section.

Discussion

A. Reaction Mechanism. We believe that a decomposition mechanism similar to that depicted above for $(CH_3O)_2Si(OH)_2$ may be operative in the decomposition of TMOS, leading to the formation of the primary products $CH_3OH + (CH_3O)_2SiOCH_2$. The $(CH_3O)_2SiOCH_2$ intermediate can undergo a carbonium ion transfer, analogous to the proton transfer in the reaction shown in Figure 9, to form $CH_3OSi(O)C_2H_5$:

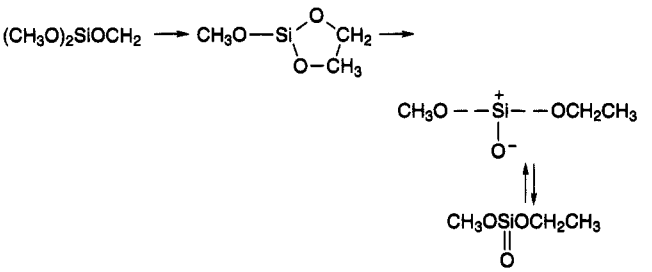

The ethyl methyl silicate thus formed is expected to decompose with facility via a four-centered transition state,[21]

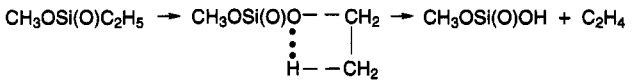

This channel is energetically more favorable than the six-centered elimination process:

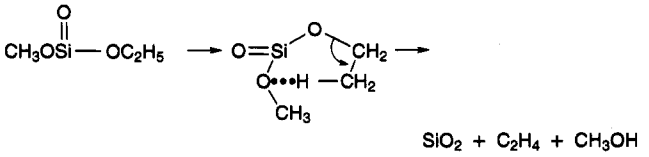

which is endothermic by as much as 80 kcal/mol.[21] The four-centered decomposition mechanism, which should be analogous to that of TEOS decomposition, is expected to have a similar first-order rate constant,[21] $k = 5 \times 10^{13} \exp(-61\,500/RT)\ s^{-1}$.

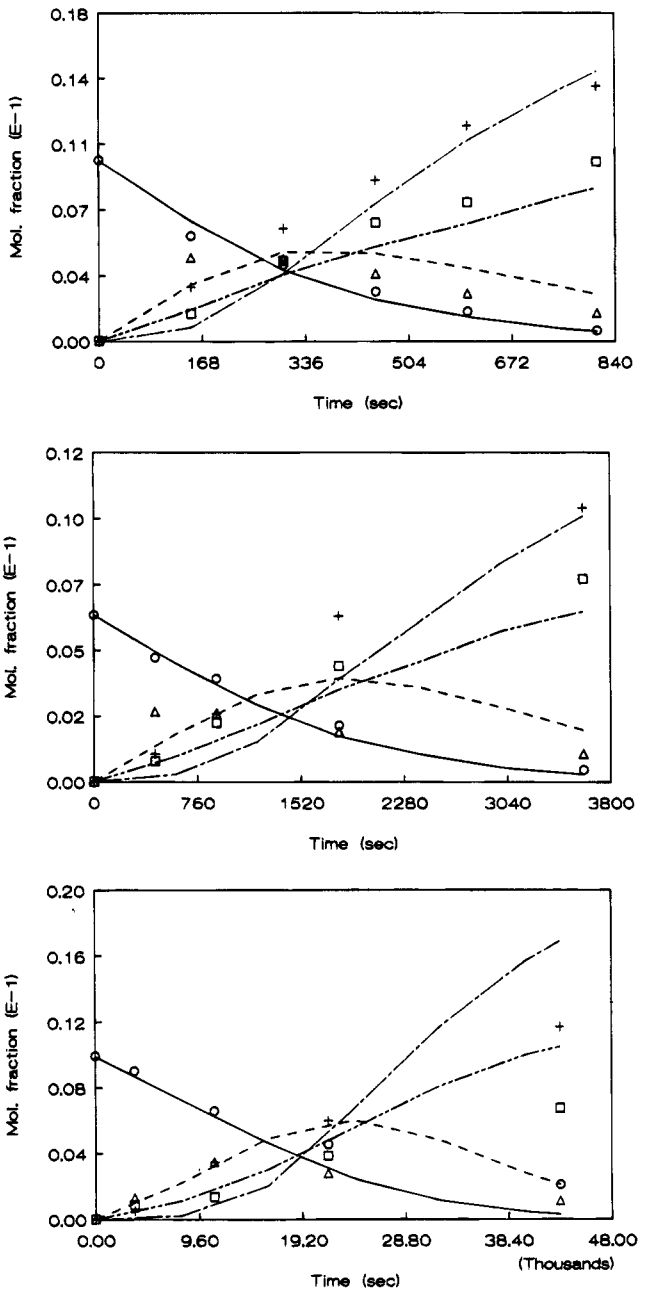

Figure 6. Concentration-time profiles of various species produced by the thermal decomposition of 0.6% TMOS in Ar without C_7H_8 at different temperatures: (a, top) 953 K; (b, middle) 915 K; (c, bottom) 858 K. The symbols represent experimental data points: (○) TMOS; (△) CH_2O; (□) CH_4; (+) CO. The curves are the results of kinetic modeling: (—) TMOS; (- -) CH_2O; (— - —) CO; (— - - —) CH_4.

It is important to note that while silicon forms strong Si—O single bonds (131 kcal/mol for CH_3O—$Si(OH)_3$ compared to 98 kcal/mol for CH_3—$OSi(OH)_3$), it forms weak Si=O double bonds, unlike carbon. Thus, for instance, we found $(HO)_2SiOCH_2$ to be as stable as $HOSi(O)OCH_3$. This effect should be true in general for the various reaction intermediates, leading to zwitterionic species, which may close to form ringed structures. These species should be extremely reactive, both in the gas phase and on surfaces. Unimolecularly, they should be able to undergo ionic rearrangement to form dative-bonded complexes (see Figures 8 and 9) which readily decompose to form products.

The results of kinetic modeling, using the mechanism given in Table 1, identify two reactions which control the overall decay of TMOS as well as the formation of the major secondary and

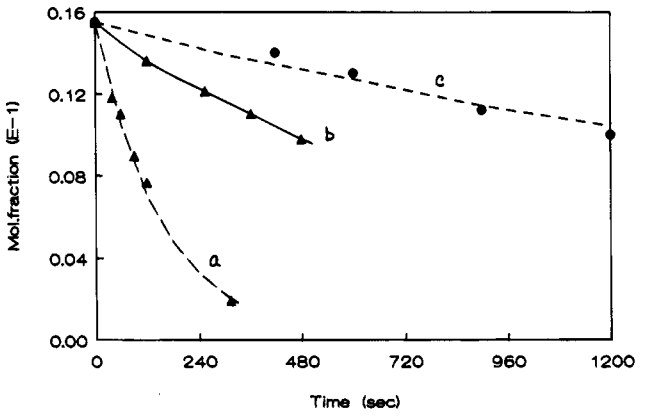

Figure 7. Concentration-time profiles of 0.16% TMOS measured in the pyrolysis of TMOS in Ar with C_7H_8 at different temperatures: (a) 984 K; (b) 918 K; (c) 866 K. The symbols represent experimental data points, and the curves are the results of kinetic modeling.

TABLE 2: Energetics of Species Relevant to the Present System Calculated by the BAC-MP4 Method

species	$\Delta H°_{f,0}$ (kcal/mol) ± estimated uncertainty
$Si(OH)_3OCH_3$	−306.8 ± 3.4
$Si(OH)_3$	−183.3 ± 1.0
$OSi(OCH_3)_2$	−170.8 ± 6.5
$CH_2OSi(OH)_3$	−262.0 ± 4.1
CH_3OSiO_2	−106.2 ± 5.2
$Si(OH)_2OCH_3$	−173.3 ± 1.0
$Si(OH)(OCH_3)_2$	−163.7 ± 1.1
$Si(OH)_2(OCH_3)_2$	−313.8 ± 3.2
c-$Si(OH)_2OCH_2$−	−180.3 ± 1.5
SiH_2OH	−22.2 ± 1.2
H_2SiO	−22.1 ± 1.0
$OSi(OH)_2$	−189.9 ± 6.2
$SiH(OH)_2$	−101.2 ± 1.2
$SiH(OH)_2O$	−158.6 ± 1.3
$SiH_2(OH)_2$	−145.7 ± 1.0
$SiH(OH)_3$	−231.1 ± 1.7
$Si(OH)_4$	−317.0 ± 3.3
$HOSiO_2$	−115.8 ± 5.0
HSiOH	−19.2 ± 2.7
$Si(OH)_3O$	−244.0 ± 3.3
H_3SiOH	−62.8 ± 1.0
$Si(OH)_2$	−113.6 ± 2.9
$OSi(OH)(OCH_3)$	−181.0 ± 6.4
SiO_2	−67.2 ± 2.1
CH_3OH	−46.2 ± 1.0
CH_3O	7.7 ± 1.3
CH_2OH	−3.2 ± 1.1
CH_3	35.6 ± 1.2
CH_2O	−25.0 ± 1.0
CH_2	92.7 ± 1.4
OH	9.5 ± 1.0
H	51.6
O	59.0

late products measured, CH_4, CH_2O, and CO.

$$(2)\ \text{TMOS} \rightarrow CH_3OH + (CH_3O)_2SiOCH_2$$

$$(3)\ CH_2OSi(OCH_3)_3 \rightarrow CH_2O + Si(OCH_3)_3.$$

Their rate constants, presented in Figures 10 and 11, respectively, can be effectively given by the following Arrhenius equations:

$$k_2 = 1.6 \times 10^{14} \exp(-74\,000/RT)\ s^{-1} \quad \text{(III)}$$

$$k_3 = 3.8 \times 10^{14} \exp(-60\,000/RT)\ s^{-1} \quad \text{(IV)}$$

The errors associated with the activation energies given above are estimated to be ±2.8 and ±4.5 kcal/mol, respectively.

TABLE 3: Dissociation Energies of Relevant Chemical Bonds Based on the Heats of Formation Given in Table 1

dissociating bond	BDE (kcal/mol)
1. H-$CH_2OSi(OH)_3$	96.4 ± 7.5[a]
2. CH_3-$OSi(OH)_3$	98.4 ± 7.9
3. CH_3O-$Si(OH)_3$	131.2 ± 5.7
4. H-$OSi(OH)_3$	124.6 ± 6.6
5. HO-$Si(OH)_3$	143.2 ± 5.3
6. O-$Si(OH)_3$	119.7 ± 4.3
7. CH_2-$OSi(OH)_3$	110.7 ± 4.8
8. CH_2O-$Si(OH)_3$	53.7 ± 4.5
9. CH_3-$OSi(OH)_2$	19.0 ± 2.2
10. CH_3O-$Si(OH)_2$	67.4 ± 2.3
11. CH_3O-$(CH_3O)Si(OH)_2$	129.0 ± 3.4
12. HO-$(OH)Si(OCH_3)_2$	140.4 ± 5.3
13. H-$OSi(O)(OH)$	125.7 ± 11.2
14. CH_3-OH	91.3 ± 3.2
15. H-CH_2OH	94.6 ± 2.1

[a] The errors were estimated by using the values given in Table 2 for the calculated heats of formation.

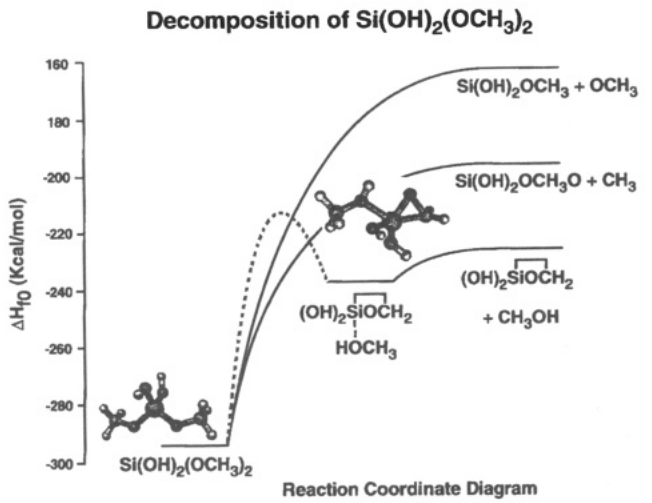

Figure 8. Schematic energy diagram for the unimolecular decomposition of $(HO)_2Si(OCH_3)_2 \rightarrow (HO)_2SiOCH_2 + CH_3OH$. The energetics were computed by the BAC-MP4 methods. The dotted curve was estimated.

In the mechanism summarized in Table 1, the unimolecular decomposition of TMOS via the radical channel

$$(1)\ \mathrm{TMOS} \rightarrow CH_3 + OSi(OCH_3)_3$$

was also included by using the thermochemical data given in Tables 2 and 3. This channel is, however, relatively unimportant except at higher temperatures. In order to account for the observed CO and CH_2O yields, the activation energy for reaction 1 was lower by about 4 kcal/mol, which is within the estimated uncertainty given in Table 2. The radicals produced from this and other decomposition processes proceed to attack the most abundant, parent molecule, resulting in a faster removal to TMOS:

$$X + \mathrm{TMOS} \rightarrow HX + CH_2OSi(OCH_3)_3$$

where X = H, OH, and CH_3. These bimolecular reactions account for the increased TMOS decay rates over those measured with toluene inhibition at higher temperatures. The scavenging effect of toluene lies in the facility of the metathetical reactions

$$X + C_6H_5CH_3 \rightarrow HX + C_6H_5CH_2$$

and the inertness of the benzyl radical, attributable to the well-known resonance stabilization effect. Because of the stability

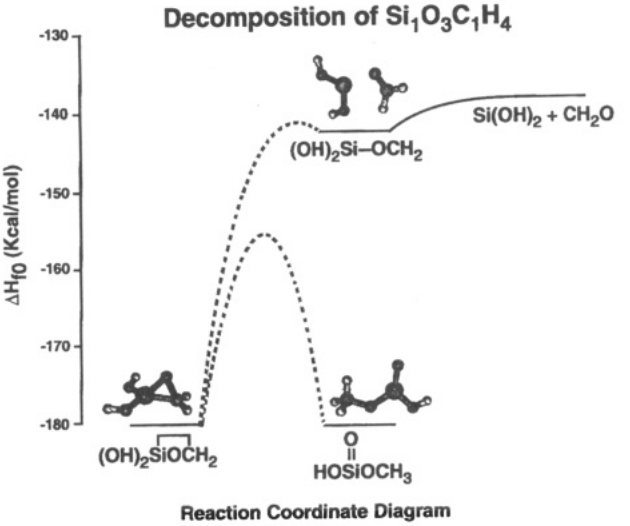

Figure 9. Schematic energy diagram for the unimolecular reaction of $(HO)_2SiOCH_2$. The energetics were computed by the BAC-MP4 method. The dotted curves were estimated.

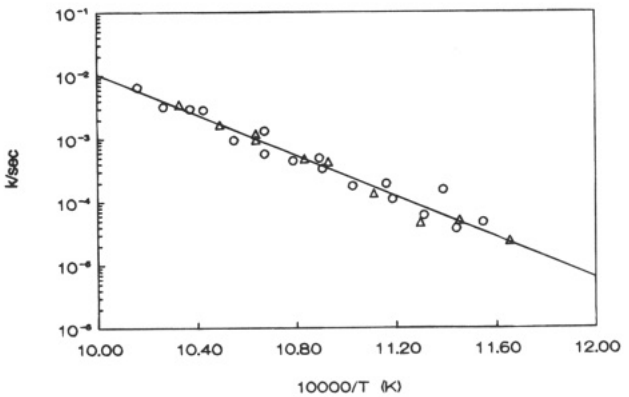

Figure 10. Arrhenius plot of the rate constant for the reaction $SiO_4C_4H_{12} \rightarrow CH_3OH + (CH_3O)_2SiOCH_2$ obtained from kinetic modeling using data from the pyrolysis of TMOS with (circles) and without (triangles) C_7H_8.

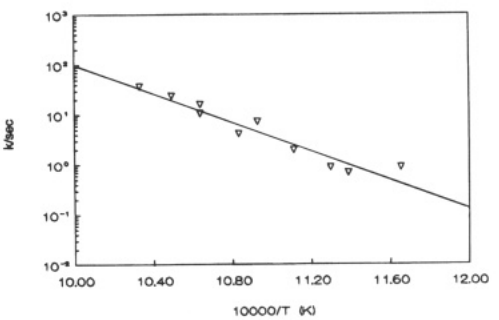

Figure 11. Arrhenius plot of the rate constant for the reaction $CH_2OSi(OC_3)_3 \rightarrow Si(OCH_3)_3 + CH_2O$. The data were obtained from experiments without C_7H_8 inhibition.

of the benzyl radical, it primarily acts as a chain terminator:

$$X + C_6H_5CH_2 \rightarrow C_6H_5CH_2X$$

which also enhances the scavenging power of toluene. The $CH_2OSi(OCH_3)_3$ radical produced by radical attacks as shown above may fragment to produce $CH_2O + Si(OCH_3)_3$ with an activation energy greater than or equal to its endothermicity (i.e., bond energy), 54 kcal/mol, as given in Table 3 using $CH_2O-Si(OH)_3$ as a model. The kinetically modeled value presented in Figure 11 is 60 ± 4.5 kcal/mol, suggesting that the barrier for the reverse reaction, $CH_2O + Si(OCH_3)_3$, is about 6 kcal/mol. This is consistent with the barrier height for H atom attack on the

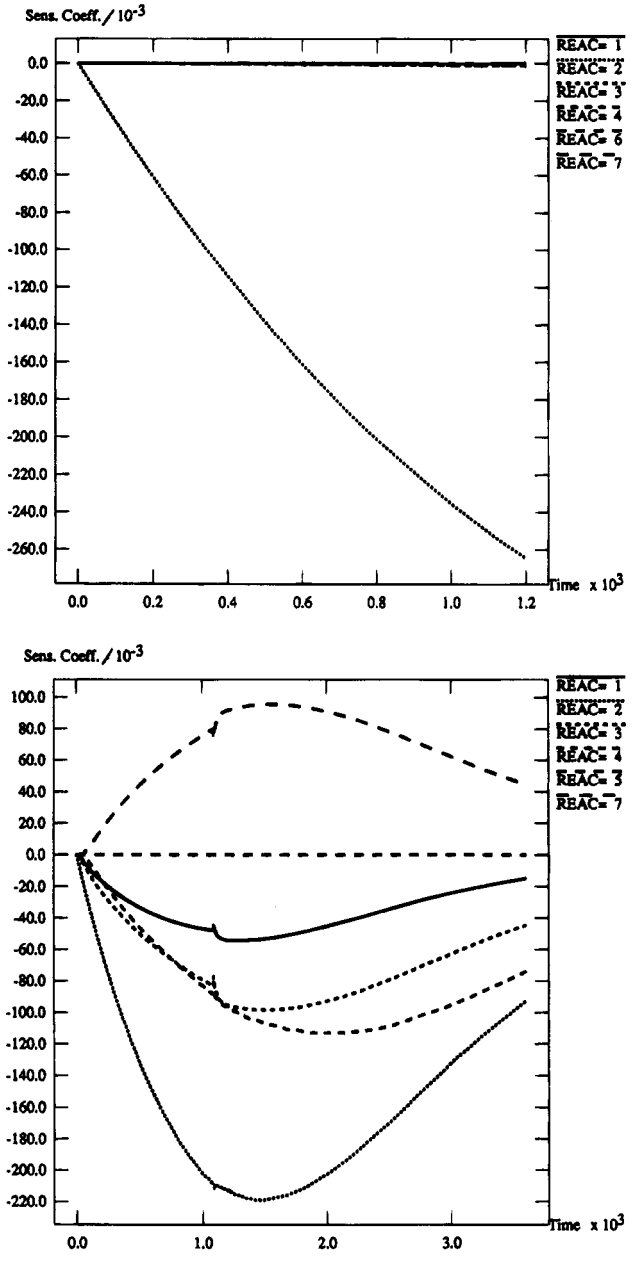

Figure 12. Sensitivity analysis for TMOS: (a, top) 0.16% TMOS + 3.2% C_7H_8 in Ar at 917 K, P = 780 Torr; (b, bottom) 0.65% TMOS in Ar at 917 K, P = 700 Torr.

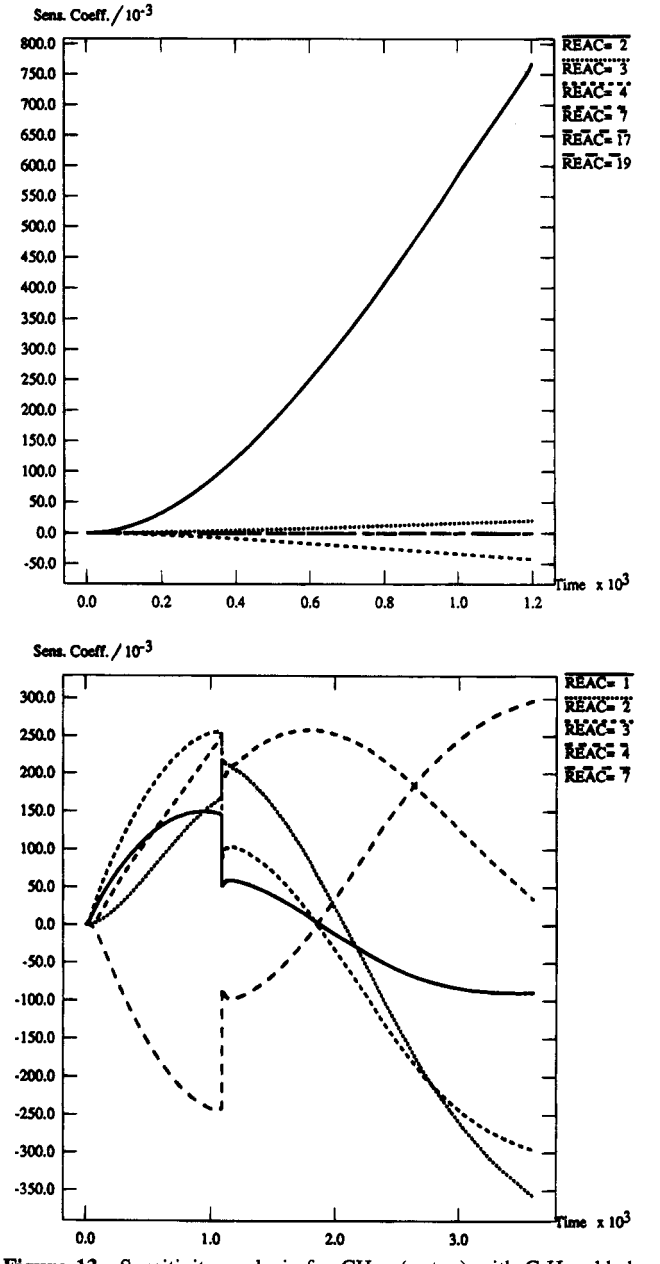

Figure 13. Sensitivity analysis for CH_4: (a, top) with C_7H_8 added; (b, bottom) without C_7H_8. Conditions are the same as given in Figure 12.

oxygen atom of CH_2O to form CH_2OH, which has a calculated BAC-MP4 barrier height of 9 kcal/mol. The result of kinetic modeling with sensitivity analysis to be discussed below indicates that the fragmentation of $CH_2OSi(OCH_3)_3$ is the major process besides the TMOS unimolecular decomposition reaction 2), which is primarily responsible for the decay of TMOS.

B. Sensitivity Analyses. The effect of any individual chemical reaction (j) on the concentration of a species of interest (i) at any time in the course of the chemical reaction can be most effectively examined by sensitivity analysis.[22] The effect can be quantified with the value of the sensitivity coefficient defined by $S_{ij} = (\delta C_i/\delta k_j)(k_j/C_i)$, where C_i is the concentration of species i and k_j is the rate constant for reaction j.

For the decay of TMOS with and without toluene inhibition, the results presented in Figure 12 qualitatively illustrate the dominant effect of reaction 2, TMOS → CH_3OH + $(CH_3O)_2SiOCH_2$. The presence of toluene effectively removes all secondary radical reactions such as reactions 3 and 4. Because of the dominant effect of reaction 2 on TMOS removal, the measured decay rates with and without the inhibitor can be used to model k_2; the modeled results are presented in Figure 10.

The yield of CH_4 also depends strongly on k_2 in the presence of toluene, but without the inhibitor, it varies in a rather complex manner with the rates of many radical reactions, most notably reactions 3 and 4 in the positive direction (i.e., $S_{ij} > 0$) and reaction 7 in the negative direction, affecting negatively its rate of production.

Similarly, CH_2O and its decomposition product, CO, were solely affected by reaction 2 in the presence of toluene; the radical reactions 3 and 4 and several others become more significant in the absence of the scavenger, as one would expect (see Figures 14 and 15).

The sharp changes in the sensitivity coefficients of CH_4, CH_2O, and CO shown in Figures 13b, 14b, and 15b, respectively, in the absence of toluene at ~1100 s resulted from the rapid increase in the rate reaction 7, H + $CH_2OSi(OCH_3)_3$, attributable to the accumulated concentrations of H and $CH_2OSi(OCH_3)_3$. The removal of these two key reactive radicals

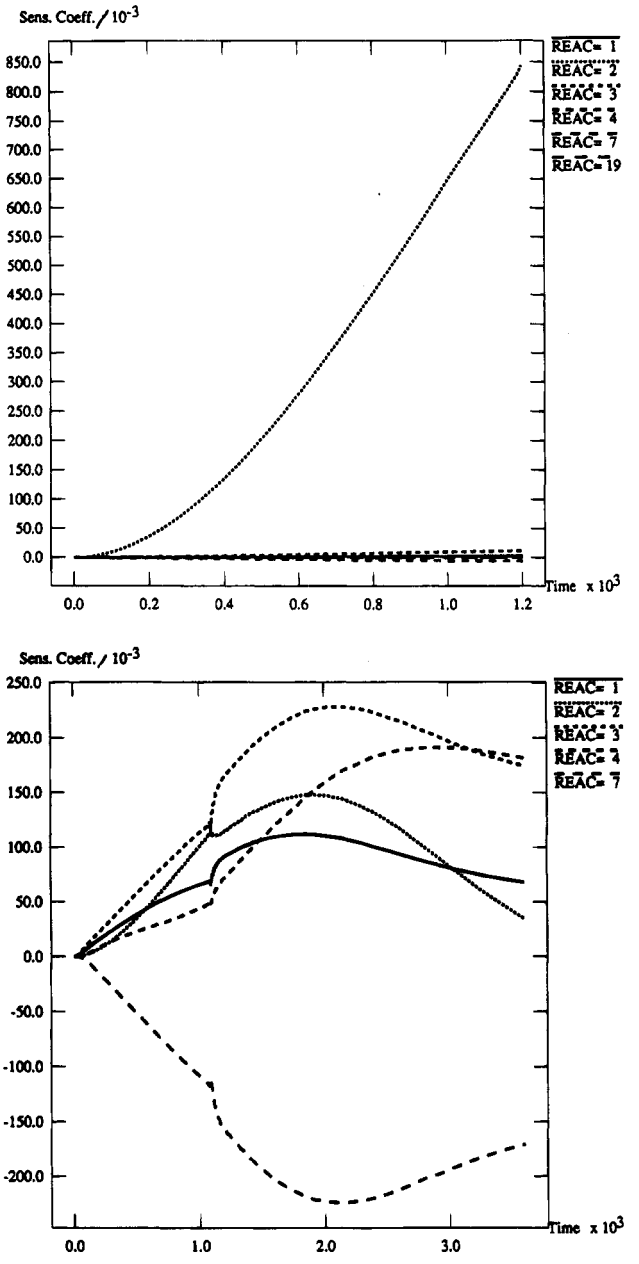

Figure 14. Sensitivity analysis for CH_2O: (a, top) with C_7H_8 added; (b, bottom) without C_7H_8. Conditions are the same as given in Figure 12.

causes a drastic effect on [H] and [CH_3], as indicated by the sensitivity analysis results. These results revealed that CH_3 was produced primarily from the chain of reactions:

$$CH_2OSi(OCH_3)_3 \rightarrow CH_2O + Si(OCH_3)_3 \quad (3)$$

$$Si(OCH_3)_3 \rightarrow O{=}Si(OCH_3)_2 + CH_3 \quad (16)$$

$$X + CH_2O \rightarrow HCO + HX \quad (X = CH_3, H) \quad (34 \text{ and } 55)$$

$$HCO + M \rightarrow CO + M \quad (35)$$

$$H + TMOS \rightarrow H_2 + CH_2OSi(OCH_3)_3 \quad (4)$$

The rapid removal of H by reaction 7 induces a drastic change in both H and CH_3 concentrations.

Conclusion

The results of the present TMOS pyrolytic study, with and without toluene inhibition, reveal that in the temperature range

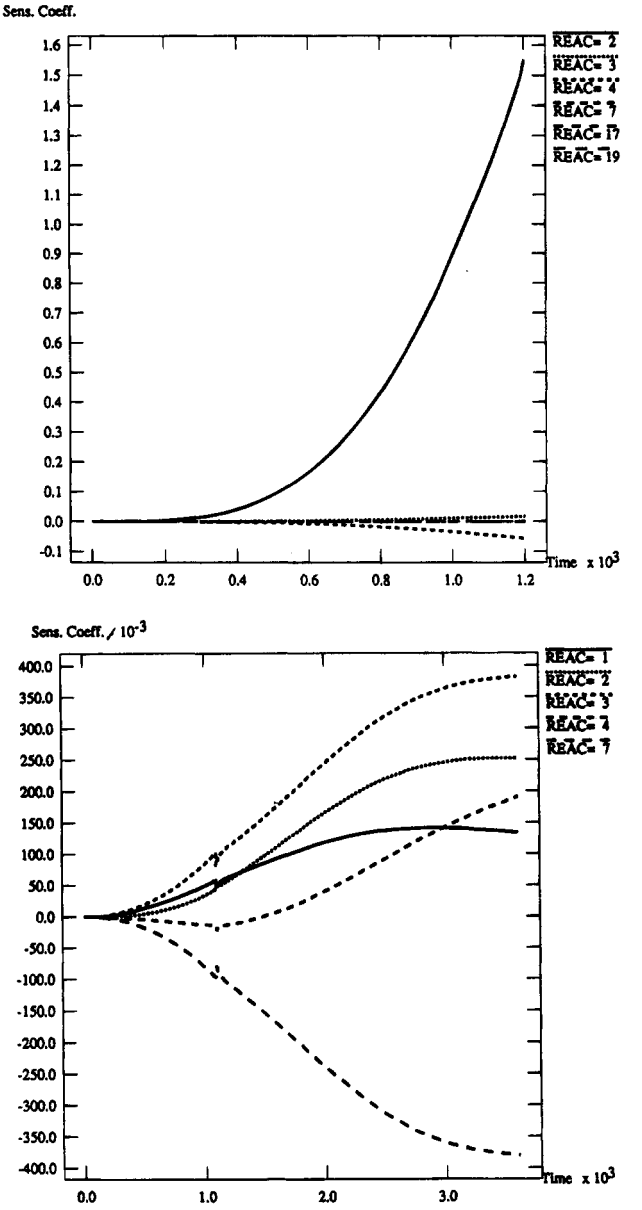

Figure 15. Sensitivity analysis for CO: (a, top) with C_7H_8 added; (b, bottom) without C_7H_8. Conditions are the same as given in Figure 12.

858−968 K the decomposition reaction takes place primarily by the unimolecular process,

$$TMOS \rightarrow CH_3OH + (CH_3O)SiOCH_2$$

with an activation energy of 74 kcal/mol. The energy barrier is substantially lower than that required for the breaking of the first C−O and Si−O bonds, 98 and 131 kcal/mol, respectively, according to the results of our quantum-chemical calculation using the BAC-MP4 technique with $(HO)_2Si(CH_3)_3$ as a model.

The quantum results also suggest the $(CH_3O)_2\overline{SiOCH_2}$ ring intermediate has a strong zwitterionic character, $(CH_3O)_2Si^+OCH_2^-$, whose enthalpy of formation is close to that of its geometric isomer, ethyl methyl silicate [$CH_3OSi(=O)OC_2H_5$], which can decompose readily to produce C_2H_4 and $CH_3OSi(O)OH$ via a four-centered transition state. The presence of a short radical chain at higher temperatures, as revealed by the effect of toluene inhibition, resulted from the decomposition of TMOS and its radical products. The attack on TMOS by the

radicals,

$$X + TMOS \rightarrow CH_2OSi(OCH_3)_3 + HX$$

generated from the fragmentation of $CH_2OSi(OCH_3O)_3$ and its radical products,

$$CH_2OSi(OCH_3)_3 \rightarrow CH_2O + Si(OCH_3)_3$$

$$Si(OCH_3)_3 \rightarrow CH_3 + O{=}Si(OCH_3)_2$$

accounts for the enhanced reaction rates and the larger A factor measured in the absence of the toluene inhibitor. The CH_2O and CH_3OH products formed in these early stages of the decomposition reaction become the important sources of the H atom:

$$X + CH_2O \rightarrow HX + CHO$$

$$CHO + M \rightarrow H + CO + M$$

$$X + CH_3OH \rightarrow HX + CH_2OH$$

$$CH_2OH + M \rightarrow CH_2O + H + M$$

The result of our sensitivity analysis indicates that the H atom is a key radical responsible for the destruction of TMOS at high temperatures. The rapid reaction of H with $C_6H_5CH_3$ accounts for the observed toluene inhibition effect.

To conclude, we should emphasize that the experimental and theoretical results presented in this paper have provided, for the first time, important thermochemical and kinetic data on TMOS and its related species (see Tables 2 and 3). The theoretically predicted fragmentation energetics for the model compound, $(HO)_2Si(OCH_3)_2$ presented in Figures 8 and 9, are consistent with the kinetically modeled activation energy for the TMOS decomposition reaction with and without toluene inhibition. In the absence of the inhibitor, the formation of secondary and tertiary products, such as CH_4, CH_2O, and CO, could be semiquantitatively accounted for with the model.

Acknowledgment. The authors gratefully acknowledge the support received from the Office of Naval Research.

References and Notes

(1) Sherman, A. *Chemical Vapor Deposition for Microelectronics*; Noyes Publications: Park Ridge, NJ, 1987.

(2) Sze, S. M. *Physics of Semiconductor Surfaces*, 2nd ed.; John Wiley and Sons: New York, 1981.

(3) Atkinson, A. *Rep. Prog. Phys.* **1985**, *37*, 231.

(4) Irene, E. A. *Crit. Rev. Solid State Mater. Sci.* **1988**, *14*, 175.

(5) Becker, F. S.; Pawlik, D.; Anzinger, H.; Spitzer, A. *J. Vac. Sci. Technol.* **1987**, *B5*, 1555.

(6) Adams, A. C.; Capio, C. D. *J. Electrochem. Soc.* **1979**, *126*, 1042.

(7) Desu, S. B. *J. Am. Ceram. Soc.* **1989**, *72*, 1615.

(8) Raupp, G. B.; Cale, T. S.; Hey, H. P. W. *J. Vac. Sci. Technol.* **1992**, *B10* (1), 37.

(9) Hertl, W. *J. Phys. Chem.* **1968**, *72*, 1248.

(10) Hertl, W. *J. Phys. Chem.* **1968**, *72*, 3993.

(11) Chu, J. C. S.; Breslin, J.; Wang, N. S.; Lin, M. C. *Mater. Lett.* **1991**, *12*, 179.

(12) Ho, P.; Melius, C. F. *J. Phys. Chem.*, submitted.

(13) Melius, C. F.; Binkley, J. S. *20th International Symposium on Combustion*; The Combustion Institute: 1984; p 575.

(14) Kee, R. J.; Miller, J. A.; Jefferson, T. H. CHEMKIN: A General-Purpose Problem-Independent, Transportable, Fortran Chemical Kinetics Code Package. Report No. SAND 80-8003; Sandia National Laboratory: Livermore, CA, 1980.

(15) Tsang, W.; Hampson, R. F. *J. Phys. Chem. Ref. Data* **1986**, *15*, 1087.

(16) Tsang, W. *J. Phys. Chem. Ref. Data* **1987**, *17*, 471.

(17) Melius, C. F. In *Chemistry and Physics of Energetic Materials*; Bulusu, S., Ed.; NATO ASI Series 209; 1990; p 21.

(18) Yang, D. L.; Yu, T.; Lin, M. C.; Melius, C. F. *J. Chem. Phys.* **1992**, *97*, 222.

(19) Ho, P.; Coltrin, M. E.; Binkley, J. S.; Melius, C. F. *J. Phys. Chem.* **1985**, *89*, 4647; **1986**, *90*, 3399.

(20) Allendorf, M. D.; Melius, C. F. *J. Phys. Chem.* **1992**, *96*, 428.

(21) Chu, J. C. S. Ph.D. dissertation, Emory University, 1993.

(22) Lutz, A. E.; Kee, R. J.; Miller, J. A. SENKIN: A Fortran Program for Predicting Homogeneous Gas Phase Chemical Kinetics with Sensitivity Analysis. Report No. SAND 87-8248; Sandia National Laboratory: Livermore, CA, 1988.

JP941927M